International Journal of Engineering Research & Technology (IJERT)
ISSN: 2278-0181
Vol. 10 Issue 11, November-2021

Simplified Dynamic Method Applied to the Study of Slope Stability

Mamba Mpele [1*], Enyegue Germain [2], Bana Abouar [3], Fry Jean Jacques[4]

[1] Professor, Department of Civil Engineering National Advanced School of Engineering, University of Yaoundé I, Cameroon. Po Box: 8390 Yaoundé – Cameroun,

[2] PhD Researcher, Department of Civil Engineering National Advanced School of Engineering, University of Yaoundé I, Cameroon.

[3]Researcher, Department of Civil Advanced School of Engineering, University of Yaoundé I, Cameroon.
[4]Embankment expert (AFPS, CFMS and CFBR)-Chambery France

***Abstract*:-The stability studies of slopes by the classical methods based on the concept of safety coefficient present some insufficiencies. They do not allow the calculation of permanent displacements induced by earth quake. To overcome this limitation, finite elements or finite volumes methods have been developed and introduced in several civil engineering calculation software. But, because the implementation of above methods is complicated, they cannot be used as a design tools but rather as a verification tool. In this paper we shows that simplified dynamic methods for the study of slopes stability under dynamic loads have been developed in the literature and their implementation is very easy, and allow the calculation of irreversible permanent displacements induced by an earthquake, which can be used as a design criterion for slopes or embankments stability.**

Key words: Embankments, stability, simplified dynamic method, earthquake.

1. INTRODUCTION

A stability study of slopes or embankments, whether natural or artificial, consists of two steps: the first one concern to geotechnical studies which permits to calculate the mechanical and physical characteristics of the soils constituting the slopes or embankments and its base. The second one is devoted to the analysis of the stability of the embankment or slope, in order to evaluate their probability of failure. This stability analysis can be performed by two methods: one probabilistic and the other determinist.

The probabilistic approach is based on the spatial uncertainties of the mechanical and physicals properties of soils, which result in an uncertainty on the representativeness of the calculation results. The implementation of this approach is very difficult and it is understandable why it is not often used by civil engineers.

On the other hand, the deterministic approach (energy methods, static and pseudo-static methods) is, with a few exceptions, systematically used. The success of this approach is explained by the fact that its implementation is based on simple theories and the obtained results are easy to interpret. However, these methods have some limitations, especially when the slopes are subjected to dynamic loads.

In this article, we will briefly review the static and pseudo-static methods of slope stability analysis, highlight some of their shortcomings and show how some of them have been overcome in the case of seismic loading.

2. DETERMINISTIC APPROACH

The deterministic approach to slope stability analysis is based on three methods:

- Energetic Methods;
- Static and Pseudo-Static Methods
- Dynamic Methods.

2.1. Energetic Methods

The objective of the energetic methods is to find the most general analytical form that can be given to the form that can be given to the normal stress function σ_n. To do this, it is assumed that there is a potential function of the failure curve and that, among all the stress distributions which verify the equations of statics, the one that makes the potential minimum is chosen. This energetic approach developed by [15] is not used by engineers. Instead, they prefer static and pseudo-static methods based on: failure calculations and the concept of the safety coefficient.

2.2. Static and pseudo-static methods

2.2.1. Concept of safety coefficient

The safety coefficient associated with a failure surface can be defined as the ratio between:

International Journal of Engineering Research & Technology (IJERT)
ISSN: 2278-0181
Vol. 10 Issue 11, November-2021

1. The maximum mobilizable tangential stress τ_{max} and the mobilized tangential stress τ on a failure surface;
2. The resisting forces and the driving forces on a failure surface
3. The resisting and driving moments of the above forces on a failure surface.

In general, the expression of τ_{max} is given by the failure criterion of Mohr Coulomb (equation 1). On the other hand, some authors, such as [15], have proposed for non-coherent materials a failure criterion given by the relation (2). The expression of the effectively mobilized stress τ is obtained by solving the equilibrium equations of the mass located above the failure line or surface.

$$\tau_{max} = c' + \sigma'_n \tan(\varphi') \quad (1)$$

$$\tau_{max} = A_0 \left(\frac{\sigma'_n}{p_{ref}} \right)^b \quad (2)$$

A_0 et $b \leq 1$ are positives coefficients ; p_{ref} the reference pressure; c' and φ' are cohesion and friction angle of soil.

The equation of the equilibrium problem of a massif is based on the following assumptions:

- The soil mass is assumed to be continuous;
- The studied problem is plane and there are no edge effects;
- The external forces are the weight of the soil, the surcharges and possibly the seismic forces. No account is taken of the driving forces that can be created by water flows;
- If there is water flow, it is not disturbed by the slopes failure and the Terzaghi's relation $\sigma = \sigma' - u$ is verified;
- The mass of the moving soil(above the line or surface failure) is assumed to be rigid and the equilibrium of this mass resting on the rest of the soil is studied;
- The seismic forces are taken into account (pseudo-static approach) by introducing the vertical k_V and horizontal k_H acceleration coefficients at the gravity center of the moving mass;
- the safety coefficient is assumed to be constant over the entire rupture area;

Based on these assumptions, the solution of the mechanical equilibrium equations can be done using: global methods or slice methods.

2.3. Slice Methods

The principle of the slice method (Figure 1) is that the moving soil mass is broken down into several small elements or slices. The individual equilibrium of each slice is studied (3). The force tensor on the unstable mass is equal to the sum of the forces applied to each slice.

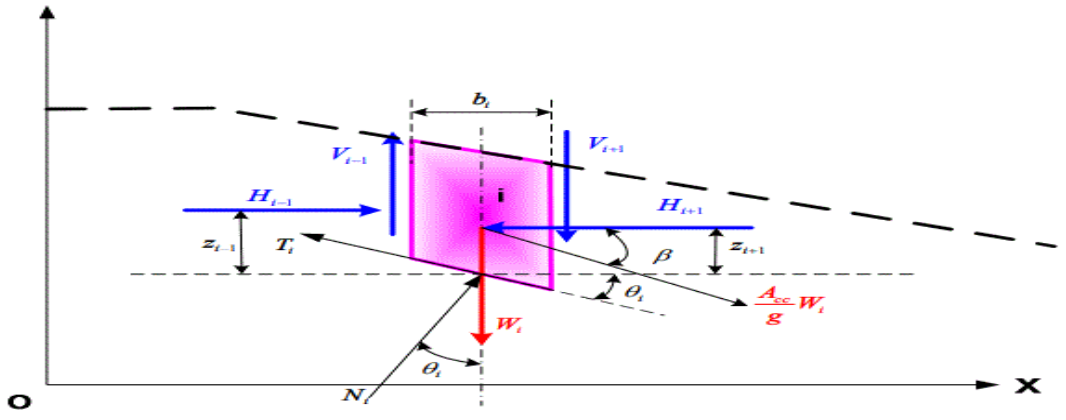

Figure 1: Forces acting on the 'i' slice

$$\begin{cases} N_i \sin(\theta_i) - T_i \cos(\theta_i) + k_H W_i + (H_{i-1} - H_{i+1}) = 0 & (a) \\ N_i \cos(\theta_i) + T_i \sin(\theta_i) - (k_V + 1) W_i + (V_{i-1} - V_{i+1}) = 0 & (b) \end{cases} \quad (3)$$

Solving the system of equations (3) gives us the following expressions for T_i and N_i

International Journal of Engineering Research & Technology (IJERT)
ISSN: 2278-0181
Vol. 10 Issue 11, November-2021

$$N_i = k_V \cos(\theta_i) W_i - k_H \sin(\theta_i) W_i + \cos(\theta_i) W_i - (V_{i-1} - V_{i+1}) \cos(\theta_i) - (H_{i-1} - H_{i+1}) \sin(\theta_i) \quad (4)$$

$$T_i = k_V \sin(\theta_i) W_i + k_H \cos(\theta_i) W_i + \sin(\theta_i) W_i - (V_{i-1} - V_{i+1}) \sin(\theta_i) + (H_{i-1} - H_{i+1}) \cos(\theta_i) \quad (5)$$

By posing:

$k_H = \frac{A_{cc}}{g} \cos(\beta)$ and $k_V = \frac{A_{cc}}{g} \sin(\beta)$, the relations (4) and (5) become:

$$N_i = \frac{A_{cc}}{g} \sin(\theta_i - \beta) W_i + \cos(\theta_i) W_i - (V_{i-1} - V_{i+1}) \cos(\theta_i) - (H_{i-1} - H_{i+1}) \sin(\theta_i) \quad (6)$$

$$T_i = \frac{A_{cc}}{g} \cos(\theta_i - \beta) W_i + \sin(\theta_i) W_i - (V_{i-1} - V_{i+1}) \sin(\theta_i) + (H_{i-1} - H_{i+1}) \cos(\theta_i) \quad (7)$$

The normal effective stress σ'_i applied to the slice "i" of width b_i is :

$$\sigma'_i \frac{b_i}{\cos(\theta_i)} = N_i - \frac{u_i b_i}{\cos(\theta_i)} \quad (8)$$

Using Mohr Coulomb's criterion $\tau_{\max_i} = c'_i + \sigma'_i \tan(\varphi'_i)$ we obtain the following expression for

$$T_{\max_i} = c'_i \frac{b_i}{\cos(\theta_i)} + \sigma'_i \frac{b_i}{\cos(\theta_i)} \tan(\varphi'_i) \quad (9)$$

The definition (F2) of the safety coefficient gives us the relation:

$$F_d = \frac{\sum_{i=1}^{n} T_{\max_i}}{\sum_{i=1}^{n} T_i} \quad (10)$$

Writing $T_{\max_i}$ as function of N_i and u_i using the expression (7) for T_i we obtain this relation (11) which gives the safety coefficient F_d :

$$F_d = \frac{\sum_{i=1}^{n} \left(c'_i \frac{b_i}{\cos(\theta_i)} + \left[-\frac{A_{cc}}{g} \sin(\theta_i - \beta) W_i + \cos(\theta_i) W_i - (V_{i-1} - V_{i+1}) \cos(\theta_i) - (H_{i-1} - H_{i+1}) \sin(\theta_i) - \frac{u_i b_i}{\cos(\theta_i)} \right] \tan(\varphi'_i) \right)}{\sum_{i=1}^{n} \left[\frac{A_{cc}}{g} \cos(\theta_i - \beta) W_i + \sin(\theta_i) W_i - (V_{i-1} - V_{i+1}) \sin(\theta_i) + (H_{i-1} - H_{i+1}) \cos(\theta_i) \right]} \quad (11)$$

Assuming that at the failure the relation (12) is verified; we obtain another expression (14) for T_i .

$$\tau_i = T_i \frac{\cos(\theta_i)}{b_i} = \frac{\tau_{\max_i}}{F_d} = \frac{c'_i + (\sigma_i - u_i) \tan(\varphi'_i)}{F_d} \quad (12)$$

$$\tau_i = \frac{c'_i + (\sigma_i - u_i) \tan(\varphi'_i)}{F_d} = \frac{c'_i + \left(\frac{N_i}{b_i} \cos(\theta_i) - u_i \right) \tan(\varphi'_i)}{F_d} \quad (13)$$

$$T_i = \frac{\left[c'_i \frac{b_i}{\cos(\theta_i)} - \frac{u_i b_i}{\cos(\theta_i)} \tan(\varphi'_i) \right] + N_i \tan(\varphi'_i)}{F_d} \quad (14)$$

By introducing the relationship (14) into equation (3b) we obtain the following expression for N_i :

International Journal of Engineering Research & Technology (IJERT)
ISSN: 2278-0181
Vol. 10 Issue 11, November-2021

$$N_i = \frac{(k_V + 1)W_i) - (V_{i-1} - V_{i+1}) - \frac{\left[c_i' - u_i \tan(\varphi_i')\right] b_i \tan(\theta_i)}{F_d}}{\left(\cos(\theta_i) + \frac{\sin(\theta_i)\tan(\varphi_i')}{F_d}\right)} \quad (15)$$

When we use relation (15) to rewrite the Mohr-Coulomb criterion, we obtain the following expression for $\tau_{\max_i}$.

$$\tau_{\max_i} = \left\{c_i' b_i - u_i b_i \tan(\varphi_i') + \left[(k_V + 1)W_i) - (V_{i-1} - V_{i+1})\right]\tan(\varphi_i')\right\} \frac{1}{b_i\left(1 + \frac{\tan(\theta_i)\tan(\varphi_i')}{F_d}\right)} \quad (16)$$

By taking the definition of the safety coefficient (D2) given by equation (17), and introducing the expressions (7), (16) of T_i and $\tau_{\max_i}$ we obtain another expression of the safety coefficient Fd which is given by relation (18).

$$F_d = \sum_{i=1}^{n}\left[\frac{\tau_{\max_i}\frac{b_i}{\cos(\theta_i)}}{T_i}\right] \quad (17)$$

$$F_d = \sum_{i=1}^{n}\left[\frac{\left\{c_i' b_i - u_i b_i \tan(\varphi_i') + \left[(k_V + 1)W_i - (V_{i-1} - V_{i+1})\right]\tan(\varphi_i')\right\}\frac{1}{\left(1 + \frac{\tan(\theta_i)\tan(\varphi_i')}{F_d}\right)\cos(\theta_i)}}{\frac{A_{cc}}{g}\cos(\theta_i - \beta)W_i + \sin(\theta_i)W_i - (V_{i-1} - V_{i+1})\sin(\theta_i) + (H_{i-1} - H_{i+1})\cos(\theta_i)}\right] \quad (18)$$

In fact;

$$\mathrm{F_d} = \begin{cases} F_s \ if \ A_{cc} = 0 \ \text{static safety coefficient,} \\ F_{ps} \ if \ A_{cc} \neq 0 \ \text{pseudo} - \text{static safety coefficient.} \end{cases}$$

2.3.1 Safety coefficient in the sense of FELLENIUS

If, $\forall\, i \geq 1\,, V_{i+1} = V_{i-1}\ and\ H_{i-1} = H_{i+1} = 0$ and using the relation (11) we obtain the pseudo-static safety coefficient of Fellenius (19).

$$F_{ps.F} = \frac{\sum_{i=1}^{n}\left(c_i' \frac{b_i}{\cos(\theta_i)} + \left[-\frac{A_{cc}}{g}\sin(\theta_i - \beta)W_i + \cos(\theta_i)W_i - \frac{u_i b_i}{\cos(\theta_i)}\right]\tan(\varphi_i')\right)}{\sum_{i=1}^{n}\left[\frac{A_{cc}}{g}\cos(\theta_i - \beta)W_i + \sin(\theta_i)W_i\right]} \quad (19)$$

And if seismic acceleration is null, we obtains a static safety coefficient of Fellenius(20).

International Journal of Engineering Research & Technology (IJERT)
ISSN: 2278-0181
Vol. 10 Issue 11, November-2021

$$F_{s.F} = \frac{\sum_{i=1}^{n}\left(c_i' \frac{b_i}{\cos(\theta_i)} + \left[\cos(\theta_i)W_i - \frac{u_i b_i}{\cos(\theta_i)}\right]\tan(\varphi_i')\right)}{\sum_{i=1}^{n}\sin(\theta_i)W_i} \quad (20)$$

2.3.2 Safety coefficient in the sense of BISHOP

If, $\forall\, i \geq 1, V_{i+1} = V_{i-1}$ *and* $H_{i-1} = H_{i+1} = 0$ and using the relation (18) we obtain the pseudo-static safety coefficient of Bishop (21).

$$F_{ps.B} = \sum_{i=1}^{n}\left[\frac{\left\{c_i' b_i - u_i b_i \tan(\varphi_i') + \left[(k_V + 1)W_i\right]\tan(\varphi_i')\right\}\frac{1}{\left(1 + \frac{\tan(\theta_i)\tan(\varphi_i')}{F_{d.B}}\right)\cos(\theta_i)}}{\frac{A_{cc}}{g}\cos(\theta_i - \beta)W_i + \sin(\theta_i)W_i}\right] \quad (21)$$

And if seismic accelerator is null, we obtain a safety static coefficient of Bishop (22).

$$F_{s.B} = \sum_{i=1}^{n}\left[\frac{\left\{c_i' b_i - u_i b_i \tan(\varphi_i') + W_i \tan(\varphi_i')\right\}}{\left(1 + \frac{\tan(\theta_i)\tan(\varphi_i')}{F_{s.B}}\right)\cos(\theta_i)}\right] \quad (22)$$
$$\sin(\theta_i)W_i$$

In the literature, there are other assumptions on the variations of : V_i , H_i and z_i which have given rise to other methods of calculating the safety coefficient: [2-4-6-8-12-21]

2.4 Global methods

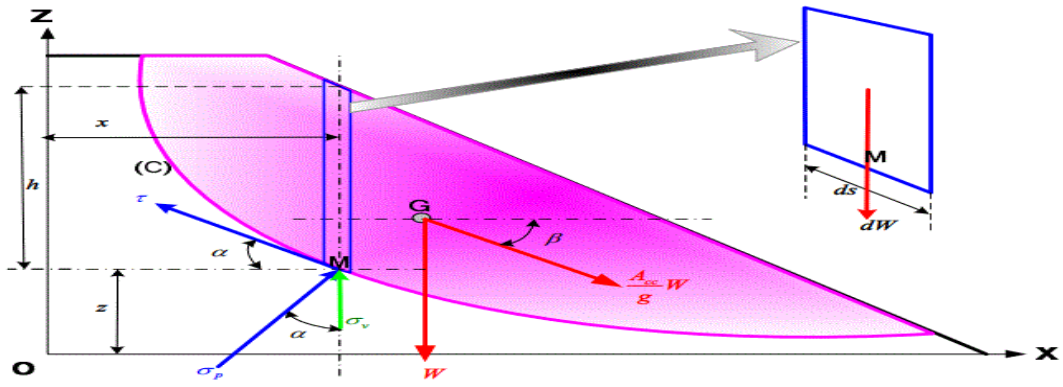

Figure 2: Global method - Massive equilibrium

The moving mass above the failure surface (C) is considered to be a rigid block and its equilibrium is studied. The equilibrium of a small element of the rigid block of center M and length ds is:

- for the equilibrium of forces:

International Journal of Engineering Research & Technology (IJERT)
ISSN: 2278-0181
Vol. 10 Issue 11, November-2021

On OX axis:

$$\int_C \left(\overrightarrow{dT} + \overrightarrow{dN}\right).\vec{i} + \int_C \overrightarrow{dW}.\vec{i} = 0 \tag{23}$$

On OZ axis:

$$\int_C \left(\overrightarrow{dT} + \overrightarrow{dN}\right).\vec{k} + \int_C \overrightarrow{dW}.\vec{k} = 0 \tag{24}$$

For the equilibrium of momentums:

$$\int_C \overrightarrow{OM} \wedge \left(\overrightarrow{dT} + \overrightarrow{dN} + \overrightarrow{dW}\right) = 0 \tag{25}$$

Using the Mohr-Coulomb's law (26) and writing the vectors $\overrightarrow{dT}, \overrightarrow{dN}$ as a function of σ_p and $\boldsymbol{\tau}$ we obtain a system of 3 equations (28) where the two unknowns are F_d and σ_p

$$\tau = \frac{c' - \left(\sigma_p - u\right)\tan\left(\varphi'\right)}{F_d} \tag{26}$$

$$\int_C \overrightarrow{dW} = \begin{bmatrix} \frac{A_{cc}}{g} W\cos(\beta) \\ -W + \frac{A_{cc}}{g} W\sin(\beta) \end{bmatrix} = \begin{bmatrix} W_1 \\ W_2 \end{bmatrix} \tag{27}$$

$$\begin{cases} \int_c \left(-\frac{c' - \left(\sigma_F - u\right)\tan\left(\varphi'\right)}{F_d} + \sigma\tan(\alpha) \right) dx = -W_1 \\ \int_c \left(\frac{c' - \left(\sigma_F - u\right)\tan\left(\varphi'\right)}{F_d}\tan(\alpha) + \sigma \right) dx = -W_2 \\ \int_c \left[\sigma_p \left(x - y\tan(\alpha)\right) + \frac{c' - \left(\sigma_F - u\right)\tan\left(\varphi'\right)}{F_d}\left(x\tan(\alpha) + y\right) \right] dx = -\int_c \left(x dW_1 - y dW_2\right) \end{cases} \tag{28}$$

To calculate the integrals of the system of equations (28), the rigid block is subdivided into several slices in order to use classical numerical integration methods. The fundamental assumption of the perturbation methods is to admit that the normal stress distribution σ_p is a function of the vertical stress σ_v applied on the horizontal facet, the parameters: c', $\Phi'$and the angle α that the tangent facet to the failure line does with the horizontal axis, where the normal stress is applied. This hypothesis, yield system of 3 equations with 3 unknowns that gave rise to the perturbation methods 1, 2 and 3 presented by [5-14].

2.5 Shortcomings of static and pseudo-static methods

The shortcomings of the static and pseudo-static methods may be found in assumptions 2, 4 and 6. Assumption 2 assumes that the slope stability problem is planar and that there are no edge effects would be partly true if the length perpendicular to the cross-section of the slope is sufficiently large compared to its width. But the dimensions of the slope being finite, it can happen that for some constructions this ratio is close to 1 (bridge piers) in which case the third dimension must be taken into account. This shortcoming led to the development of 3D stability methods by [1-11-22] , Hypothesis 4, states that shear does not cause change in pore pressures at the failure surface. This statement, which is contradicted by the work of [19] has led to the development of slope stability methods that take into account pore pressure variations during shear. Hypothesis 6, which characterizes pseudo-static methods, attempts to take into account the effect of earthquakes by introducing seismic acceleration coefficients. This method is not applicable for the analysis of soil masses with a risk of liquefaction and its major problems are:

International Journal of Engineering Research & Technology (IJERT)
ISSN: 2278-0181
Vol. 10 Issue 11, November-2021

- The choice of seismic coefficients which seems arbitrary, although some authors such as [7-18] have proposed their maximum values as a function of: Magnitude, focal distance and soil type.
- From a theoretical point of view, this method is not satisfactory because the dynamic nature of the seismic action is not taken into account: the eigen periods of the slope are not known and the induced permanent displacements are not calculated although they are used as a second (the first being stress-based) stability study criterion in most engineering problems.

In the end, all the methods mentioned above, have been established on the principle of limits state of resistance calculation. The fact of having a safety coefficient lower than 1 must therefore be interpreted as the resistant forces being exceeded by driving forces (criterion of not exceeding the constraints violated). The second criterion for not exceeding a threshold displacement value, is also important in the dynamic design of geostructures (dams and embankments) with elastoplastic behavior (due to the existence of induced permanent displacements). For embankments, Simplified Dynamic Methods developed by [10-13], , were often used in the literature for the verification and dynamic pre-design of embankments or dams: Dynamic embankment design tools based on these methods have been developed by : [3-9-20]. In the following pages basics of this method will be presented here.

3. Simplified Dynamic Methods

3.1 Principle

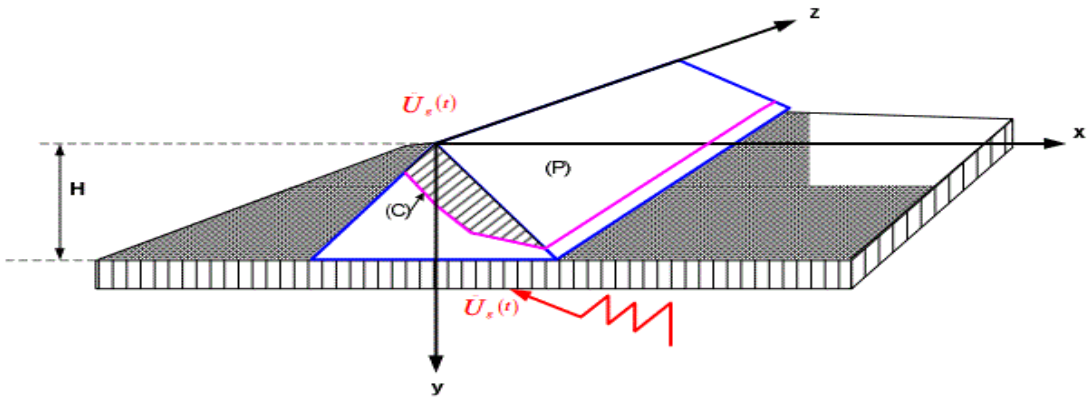

Figure 3: Infinitely long embankment under seismic loading

The principle of the simplified dynamic methods is based on the analysis of the elastic response of a homogeneous triangular or trapezoidal embankment of height "H", based on a rigid foundation subjected to the action of the seismic acceleration $\ddot{U}_g(t)$. At the end of this analysis the natural frequencies W_n, the maximum distortion γ_{max} of the embankment as well as the maximum accelerations $\ddot{U}_{max}$, k_{max} applied at the crest of the embankment and on the unstable part of the embankment (P) above the failure surface (C) are calculated.

The critical acceleration k_c associated with the failure surface (C) is then compared to the maximum average acceleration k_{max} applied (Figure 3) to the unstable part (P):

- If $\frac{K_c}{K_{max}} \geq 1$ the unstable part (P) of the embankment (Figure 3) does not move (or is stable);

- If $\frac{K_c}{K_{max}} \prec 1$ he unstable part (P) of the dam (Figure 3) moves along the failure surface. This displacement must be estimated

in order to compare it to the values of the admissible displacements tolerated by the project owner.

The knowledge of these parameters requires that a study of the elastic response of an embankment under dynamic loading be carried out.

International Journal of Engineering Research & Technology (IJERT)
ISSN: 2278-0181
Vol. 10 Issue 11, November-2021

3.2 Elastic response of an embankment under dynamic loading

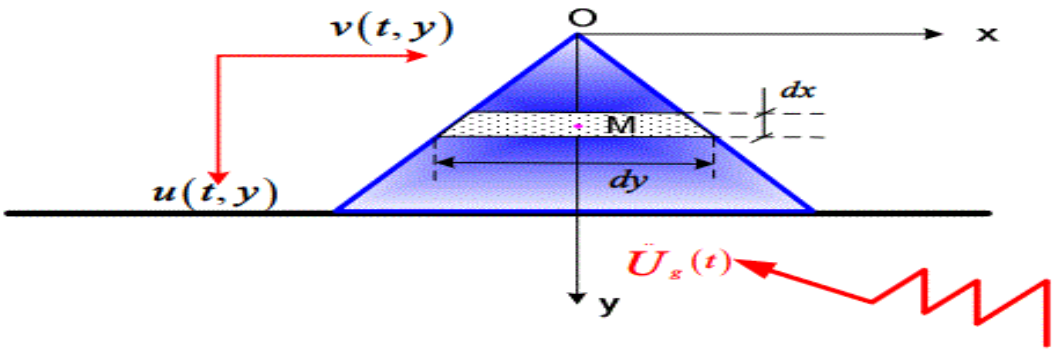

Figure 4: Modelling of [19]

The study of the elastic response of an embankment (Figure 4) under dynamic loading by [9-10-13] is based on the following four assumptions:

1. the material of the embankment body is homogeneous and its mechanical behavior is governed by a linear elastic law;
2. the influence of stored water is negligible, no significant loss of strength in relation to the generation of pore pressures;
3. the embankment is infinitely long and modelled by an infinite number of thin horizontal slices interconnected by an elastic spring system;
4. the mechanical problem considered is the planar type.

According to this model, the equations of motion governing the free vibrations of the [9] embankment (Figure 4) are:

$$\begin{cases} \dfrac{\partial^2 u}{\partial t^2} - \dfrac{G}{\rho}\left(\dfrac{\partial^2 u}{\partial y^2} + \dfrac{1}{y}\dfrac{\partial u}{\partial y}\right) = 0 \\ \dfrac{\partial^2 v}{\partial t^2} - \dfrac{\lambda^0 + 2G}{\rho}\left(\dfrac{\partial^2 v}{\partial y^2} + \dfrac{1}{y}\dfrac{\partial v}{\partial y}\right) = 0 \end{cases} \tag{29}$$

Where ρ, G and $\lambda^0 = \dfrac{\nu E}{(1-2\nu)(1+\nu)}$ are: density, shear modulus and lame coefficient of the embankment material.

$u(t,y), v(t,y)$ vertical and horizontal displacement of point M (Figure 4).Under the effect of the earthquake, equation (29) after adding the second member gives the system of equation (30) :

$$\begin{cases} \dfrac{\partial^2 u}{\partial t^2} - \dfrac{G}{\rho}\left(\dfrac{\partial^2 u}{\partial y^2} + \dfrac{1}{y}\dfrac{\partial u}{\partial y}\right) = -\dfrac{\partial^2 u_g}{\partial t^2} \\ \dfrac{\partial^2 v}{\partial t^2} - \dfrac{\lambda^0 + 2G}{\rho}\left(\dfrac{\partial^2 v}{\partial y^2} + \dfrac{1}{y}\dfrac{\partial v}{\partial y}\right) = -\dfrac{\partial^2 v_g}{\partial t^2} \end{cases} \tag{30}$$

International Journal of Engineering Research & Technology (IJERT)
ISSN: 2278-0181
Vol. 10 Issue 11, November-2021

Where $\frac{\partial^2 u_g}{\partial y^2}$ and $\frac{\partial^2 v_g}{\partial y^2}$ represent the horizontal and vertical component of the acceleration transmitted to the foundation soil by the acceleration earthquake $\overrightarrow{\ddot{U}_g(t)}$. By using $\xi = \frac{y}{H}$ we obtain the following equations system (31).

$$\begin{cases} \dfrac{\partial^2 u}{\partial t^2} - \dfrac{G}{\rho H^2}\left(\dfrac{\partial^2 u}{\partial \xi^2} + \dfrac{1}{\xi}\dfrac{\partial u}{\partial \xi}\right) = -\dfrac{\partial^2 u_g}{\partial t^2} \\ \dfrac{\partial^2 v}{\partial t^2} - \dfrac{\lambda^0 + 2G}{\rho H^2}\left(\dfrac{\partial^2 v}{\partial \xi^2} + \dfrac{1}{\xi}\dfrac{\partial v}{\partial \xi}\right) = -\dfrac{\partial^2 v_g}{\partial t^2} \end{cases} \tag{31}$$

The solutions of the system of equation (31) according to [19] are in the form:

$$\begin{cases} u(t,\tau) = \sum_{n=1}^{\infty} \dfrac{2 j_0(\beta_n \xi)}{\omega_n^0 \beta_n j_1(\beta_n)} \int_0^t \dfrac{\partial^2 u_g(\tau)}{\partial t^2} \sin\left(\omega_n^0 (t-\tau)\right) d\tau \\ v(t,\tau) = \sum_{n=1}^{\infty} \dfrac{2 j_0(\beta_n \xi)}{\omega_n^1 \beta_n j_1(\beta_n)} \int_0^t \dfrac{\partial^2 v_g(\tau)}{\partial t^2} \sin\left(\omega_n^1 (t-\tau)\right) d\tau \end{cases} \tag{32}$$

Where:

$$\begin{cases} \omega_n^0 = \beta_n \sqrt{\left(\dfrac{G}{\rho H^2}\right)} \\ \omega_n^1 = \beta_n \sqrt{\left(\dfrac{\lambda^0 + 2G}{\rho H^2}\right)} = \omega_n^0 \sqrt{2 + \dfrac{\lambda^0}{G}} \end{cases} \tag{33}$$

w_n^0 and w_n^1 denotes the n[th] horizontal and vertical natural frequency of the embankment

j_0 and j_1 are the Bessel functions of order zero and one. β_n the n[th] root of the Bessel function j_0 The first three values of β_n are:

$$\begin{cases} \beta_1 = 2.4048 \\ \beta_2 = 5.5201 \\ \beta_3 = 8.653 \end{cases} \tag{34}$$

If we introduce the damping of order λ_n, using the fact that it is much less than 1, the relations (32) become:

$$\begin{cases} u(t,\tau) = \sum_{n=1}^{\infty} \dfrac{\Phi_n(\xi)}{\omega_n^0} \int_0^t \dfrac{\partial^2 u_g(\tau)}{\partial t^2} \exp\left(-\lambda_n \omega_n^0 (t-\tau)\right) \sin\left(\omega_n^0 (t-\tau)\right) d\tau \\ v(t,\tau) = \sum_{n=1}^{\infty} \dfrac{\Phi_n(\xi)}{\omega_n^1} \int_0^t \dfrac{\partial^2 v_g(\tau)}{\partial t^2} \exp\left(-\lambda_n \omega_n^1 (t-\tau)\right) \sin\left(\omega_n^1 (t-\tau)\right) d\tau \end{cases} \tag{35}$$

Where $\Phi_n(\tau) = \dfrac{2 j_0(\beta_n \tau)}{\beta_n j_1(\beta_n)}$ And then we put $U^{\alpha}(\tau,t) = \begin{cases} u(\tau,t) \ si \ \alpha = 0 \\ v(\tau,t) \ si \ \alpha = 1 \end{cases}$

International Journal of Engineering Research & Technology (IJERT)
ISSN: 2278-0181
Vol. 10 Issue 11, November-2021

3.2.1 Relative acceleration at a point on the embankment

The relative acceleration at time t and at a point M on the coast $\xi = \frac{y}{H}$ of the embankment is:

$$\frac{\partial^2 U^{\alpha}(t,\xi)}{\partial t^2} = \sum_{n=1}^{\infty}\left(\omega_n^{\alpha}\right)^2 \cdot U_n^{\alpha}(t,\xi) = \sum_{n=1}^{\infty}\left(\omega_n^{\alpha}\right)^2 .\Phi_n(\xi)\cdot V_n^{\alpha}(t) \quad (36)$$

Where $V_n^{\alpha}(t) = \int_0^t \ddot{U}_g^{\alpha}(\zeta)\exp\left(-\lambda_n\omega_n^{\alpha}(t-\zeta)\right)\sin\left(\omega_{dn}^{\alpha}(t-\zeta)\right)d\zeta$ (37)

The velocity V_n^{α} associated with the mode n is, according to Mamba [19], a convolution integral which depends on: the relative acceleration $\ddot{U}_g^{\alpha}(t)$ and, the damping λ_n and the natural frequency w_n. For a given $\ddot{U}_g^{\alpha}(t)$ and "n", $V_n^{\alpha}(t)$ has a maximum called spectral velocity. The associated spectral acceleration S_{an}^{α} is then equal to: $S_{an}^{\alpha} = w_n^{\alpha}.S_{vn}^{\alpha}$

Finally the maximum acceleration at any point $\xi = \frac{y}{H}$ of the embankment is:

$$\ddot{U}_{\max}^{\alpha}(\xi) = \sqrt{\sum_{n=1}^{\infty}\left(\omega_n^{\alpha}\Phi_n(\xi)S_{vn}^{\alpha}\right)^2} \quad (38)$$

$$\ddot{U}_{\max}^{\alpha}(\xi) = \sqrt{\sum_{n=1}^{\infty}\left(\Phi_n(\xi)S_{an}^{\alpha}\right)^2}$$

The maximum acceleration at the embankment crest $\xi = \frac{y}{H} = 0$ has the expressions:

$$\ddot{U}_{\max}^{\alpha} = \sqrt{\sum_{n=1}^{\infty}\left(\omega_n^{\alpha}\Phi_n(0)S_{vn}^{\alpha}\right)^2} \quad (39)$$

$$\ddot{U}_{\max}^{\alpha} = \sqrt{\sum_{n=1}^{\infty}\left(\Phi_n(0)S_{an}^{\alpha}\right)^2} \quad (40)$$

$$\ddot{U}_{\max}^{\alpha} = \sum_{n=1}^{\infty}\left(\omega_n^{\alpha}\right)^2 .U_{\max}^{\alpha} \quad (41)$$

3.2.2 Relative distortion at a point on the embankment

The distortion caused by the relative displacement U^{α} at a point M of the embankment located at the coast $\xi = \frac{y}{H}$ is given by:

International Journal of Engineering Research & Technology (IJERT)
ISSN: 2278-0181
Vol. 10 Issue 11, November-2021

$$\gamma^{\alpha}(t,\xi)=\frac{1}{H}\frac{\partial U^{\alpha}(t,\xi)}{\partial \xi} \tag{42}$$

Reasoning in the same way as in the previous paragraph we obtain the following relationship of distortion:

$$\gamma^{\alpha}(t,\xi)=\frac{H}{\left(v_s^{\alpha}\right)^2}\sum_{n=1}^{\infty}\omega_n^{\alpha}V_n^{\alpha}(t)\frac{\partial\Phi_n(\xi)}{\partial\xi} \tag{43}$$

Let's pose $\gamma^{\alpha}(t,\xi)=\begin{cases}\text{distortion if } \alpha=0\\ \text{settlement if } \alpha=1\end{cases}$

Whatever the time t, the maximum distortion at a point M located at the coast $\xi=\frac{y}{H}$ in the embankment is:

$$\gamma_{\max}^{\alpha}(\xi)=\frac{H}{\left(v_s^{\alpha}\right)^2}\sqrt{\sum_{n=1}^{\infty}\left(S_{an}^{\alpha}\frac{\partial\Phi_n(\xi)}{\partial\xi}\right)^2} \tag{44}$$

Where V_s^{α} represents the wave velocity in the embankment: α=0 if the velocity is horizontal and 1 if it is vertical.

$$v_s^{\alpha}=\begin{cases}\sqrt{\frac{G}{\rho}} \text{ if } \alpha=0\\ \sqrt{\frac{\lambda^0+2G}{\rho}} \text{ if } \alpha=1\end{cases} \tag{45}$$

3.2.3 Maximum acceleration applied to the unstable part (P) of the embankment

In the following, it is assumed that the seismic stress is a pure shear wave (Figure 5). This means that $\alpha=0$

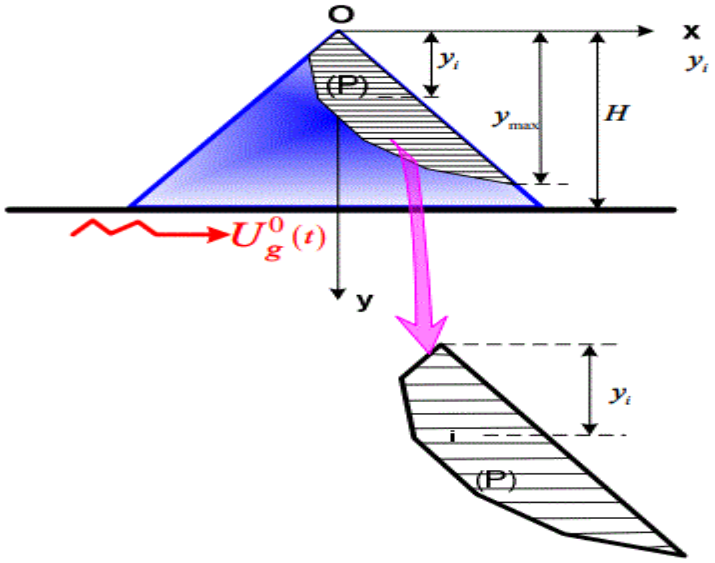

Figure 5: Principle of calculation of the acceleration applied to the part (P)

International Journal of Engineering Research & Technology (IJERT)
ISSN: 2278-0181
Vol. 10 Issue 11, November-2021

The acceleration applied at any point of the unstable part (P) of the embankment located above the failure line and assumed to be rigid is: $\ddot{U}^0(\xi) \ \forall \xi \in (P)$

If **W** is the weight of the unstable part (P) which has been divided into "n" slices. If $dm(y_i)$ is the elementary mass of the slice "i" located at the coast "y". The average acceleration applied on the part (P) of the embankment is:

$$k_{moy}(t,\xi).g = \frac{g}{W}\sum_{i=1}^{n}\left[dm(y_i).\ddot{U}^0(t,\xi_i)\right] \tag{46}$$

$$k_{moy}\left(t,\frac{y_{\max}}{H}\right) = \frac{1}{W}\sum_{y=0}^{y=y_{\max}}\left[dm(y).\ddot{U}^0\left(t,\frac{y}{H}\right)\right] \tag{47}$$

And its integral form is given by the expression (48).

$$k_{moy}\left(t,\frac{y_{\max}}{H}\right) = \frac{1}{W}\int_0^{y_{\max}}\ddot{U}^0\left(t,\frac{y}{H}\right)dm(y) \tag{48}$$

The maximum average acceleration coefficient k_{max} applied to the gravity center (stiffness assumption) of the unstable part (P) of the embankment is:

$$k_{\max} = Max\left[k_{moy}\left(t,\frac{y_{\max}}{H}\right)\right] \tag{49}$$

In all that follows we assume:

$$K_c = k_c.g\,,\ K_{\max} = k_{\max}.g \ \text{ et } \ \ddot{U}_{\max} = \ddot{u}_{\max}.g \tag{50}$$

Based on the study of the elastic response of embankments under seismic loading, simplified dynamic methods have been developed by several authors:[10-13-16]. In this article we will only present the Makdisi and Seed's method.

4. MAKDISI AND SEED'S METHOD

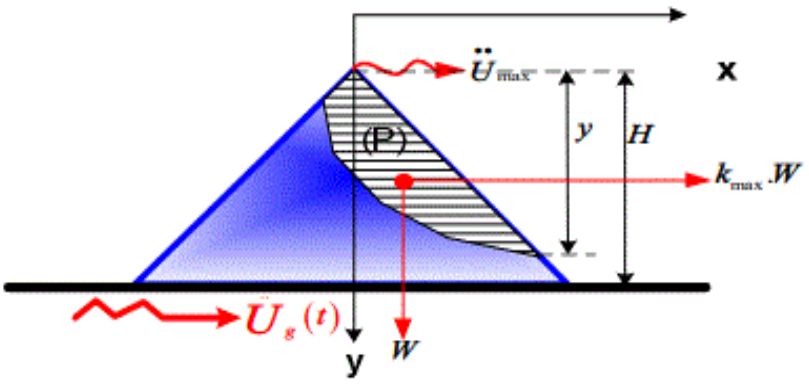

Figure 6: Solicitation according to [10]

In the of Makdisi and Seed's method, it is assumed that the seismic loading is a pure shear wave. The solutions sought are those

International Journal of Engineering Research & Technology (IJERT)
ISSN: 2278-0181
Vol. 10 Issue 11, November-2021

obtained previously provided that α = 0. Let be:

$$\ddot{U}_g^0(t,\xi), \ddot{U}^0(t,\xi) \ , \ \gamma_{\max}^0(\xi), S_{an}^0 \tag{51}$$

$$\ddot{U}_{\max}^0(0) = \ddot{U}_{\max} = \sqrt{\sum_{n=1}^{\infty}\left(\Phi_n(0) S_{an}^0\right)^2} \tag{52}$$

$$\gamma_{\max}^0(\xi) = \gamma_{\max}(\xi) = \frac{H}{\left(v_s^{\alpha}\right)^2}\sqrt{\sum_{n=1}^{\infty}\left(S_{an}^0 \frac{\partial \Phi_n(\xi)}{\partial \xi}\right)^2} \tag{53}$$

$$S_{an}^0 = w_n^0 . S_{vn}^0, \ S_{vn}^0 = Max\left[V_n^0(t)\right] \tag{54}$$

$$V_n^0(t) = \int_0^t \ddot{U}_g^0(\zeta)\exp\left(-\lambda_n \omega_n^0(t-\zeta)\right)\sin\left(\omega_{dn}^0(t-\zeta)\right)d\zeta \tag{55}$$

$$\begin{cases} \beta_1 = 2.4048 \\ \beta_2 = 5.5201 \\ \beta_3 = 8.653 \end{cases} \quad et \quad w_n^0 = \frac{\beta_n}{H}\sqrt{\left(\frac{G}{\rho}\right)} \tag{56}$$

4.1 Makdisi Seed Approximations

An observation by [29], of the evolution of the functions $\phi_n(\xi)$ as a function of ξ allowed:

1. to neglect the contribution of modes greater than 3, for the calculation of the maximum peak acceleration $\ddot{U}_{max}$;
2. To neglect the contribution of modes greater than 1, for the calculation of the maximum distortion $\gamma_{\max}^0(\xi)$;
3. Consider that the equivalent cyclic distortion $\gamma_{\text{cycl}}^{eq}(\xi)$ is equal to 0.65 times the value of the mean distortion and that $[\dot{\phi}_1(0)]_{moy} \neq 0{,}3$;
4. Consider that the dynamic shear modulus and the damping of the embankment material are functions of the cyclic distortion. a result of these approximations, we deduce the following relationships:

$$\ddot{U}_{\max}^0(0) = \ddot{U}_{\max} = \left[\sum_{i=1}^{3}\left(\Phi_i(0) S_{ai}\right)^2\right]^{0,5} \tag{57}$$

$$\gamma_{\max}^0(\xi) = \gamma_{\max}(\xi) = \frac{H}{\left(V_s\right)^2}\dot{\Phi}_1 . S_{a1} \tag{58}$$

$$\gamma_{cycl}^{eq}(\xi) = 0{,}65\left[\gamma_{\max}(\xi)\right]_{moy} = 0{,}65\frac{H}{\left(V_s\right)^2}.S_{a1}\left[\dot{\Phi}_1\right]_{moy} \tag{59}$$

$$\gamma_{cycl}^{eq}(\xi) = 0{,}195\frac{H}{\left(V_s\right)^2}.S_{a1} \tag{60}$$

International Journal of Engineering Research & Technology (IJERT)
ISSN: 2278-0181
Vol. 10 Issue 11, November-2021

$$\ddot{U}_{\max} = \left[\left(1,6.S_{a1}\right)^2 + \left(1,06.S_{a2}\right)^2 + \left(0,86.S_{a3}\right)^2 \right]^{0,5} \quad (61)$$

$$\Phi_1(0) = 1,6 \quad \Phi_2(0) = 1,06 \quad \Phi_1(0) = 0,86$$

Using the [23] hypothesis based on the mechanical rigid plastic behavior of the soil and on the basis of the results of cyclic laboratory tests [10], calculated for different accelerations, the permanent displacements induced by earthquakes of magnitude **6,5**; **7,5**; **8.25** and the whole results are presented as curves representing the ratio $\frac{y}{H}$ versus $\frac{K_{max}}{\ddot{U}_{max}}$ Figure (7) and then normalized time $\frac{d}{k_{max}\ .g.T_0}$ versus Magnitude and ratio $\frac{k_c}{k_{max}}$ (Figure 8) which are used as charts.If ***d*** denotes the value of the permanent displacement induced along the failure surface; the variables $\ddot{U}_{max}, k_c, g, T_0, H \text{ and } k_{max}$ represent respectively: the maximum acceleration at the embankment crest, the critical acceleration, the acceleration of gravity, the first mode period of the embankment, the height of the embankment and the maximum average acceleration applied on its unstable part. The ratios: $\frac{y}{H}$ The ratios: $\frac{K_{max}}{\ddot{U}_{max}}, \frac{k_c}{k_{max}}$ are unit less numbers and ***d*** is in meters when g is $\mathbf{m.s^{-1}}$, T_0 in second and k_{max} unit less coefficient for the maximum acceleration of the unstable part of the embankment.

Figures (7) and (8) show the charts of [19] and with a minimum correlation coefficient of 99% [19] proposed the relationships 62 to 67 which can be used instead of the charts.

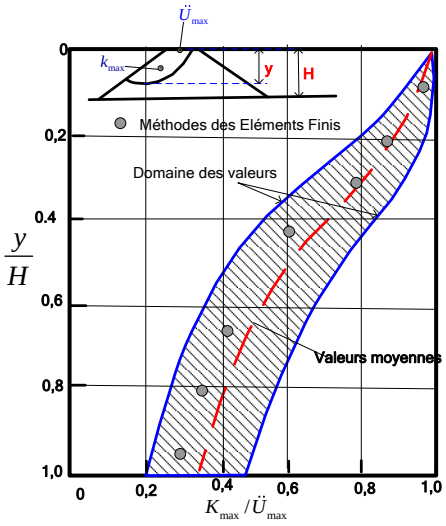

Figure 7: Ratio of maximum accelerations to depth of sliding mass according to [10]

International Journal of Engineering Research & Technology (IJERT)
ISSN: 2278-0181
Vol. 10 Issue 11, November-2021

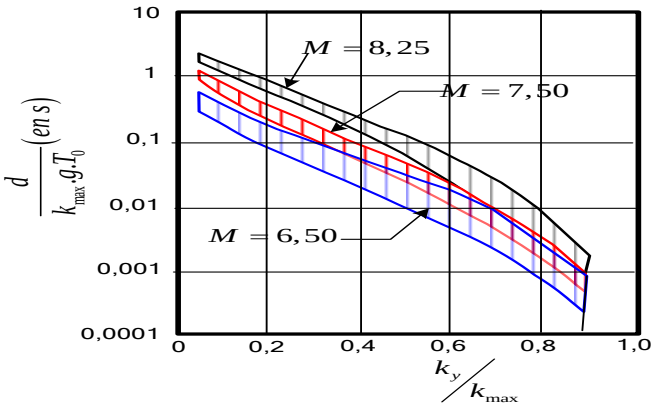

Figure 8: Average values of normalized displacement as a function of magnitude and the ratio of critical to maximum acceleration of the unstable block according to [10]

$$\left(\frac{k_{\max}}{\ddot{U}_{\max}}\right)_{\max} = f_1\left(\frac{y}{H}\right) = \begin{cases} 1 \text{ si } \dfrac{y}{H} = 0 \\ 1,07\exp\left(-0,37261\left(\dfrac{y}{H}\right)^2 - 0,492\dfrac{y}{H}\right) \text{ si } 0 < \dfrac{y}{H} \le 1 \end{cases} \tag{62}$$

$$\left(\frac{k_{\max}}{\ddot{U}_{\max}}\right)_{moy} = f_2\left(\frac{y}{H}\right) = \begin{cases} 1 \text{ si } \dfrac{y}{H} = 0 \\ 1,08\exp\left(-0,221\left(\dfrac{y}{H}\right)^2 - 0,985\dfrac{y}{H}\right) \text{ si } 0 < \dfrac{y}{H} \le 1 \end{cases} \tag{63}$$

$$\left(\frac{k_{\max}}{\ddot{U}_{\max}}\right)_{\min} = f_4\left(\frac{y}{H}\right) = \begin{cases} 1 \text{ si } \dfrac{y}{H} = 0 \\ 1,117\exp\left(0,142\left(\dfrac{y}{H}\right)^2 - 1,914\dfrac{y}{H}\right) \text{ si } 0 < \dfrac{y}{H} \le 1 \end{cases} \tag{64}$$

For $0,1 \prec \dfrac{k_c}{k_{\max}} \le 0,7$

Magnitude earthquake 8.25 (average values) :

$$\frac{d}{k_{\max}.g.T_0} = \exp\left[-3,674 - 1,596Ln\left(\frac{k_c}{k_{\max}}\right) - 11,615\left(\frac{k_c}{k_{\max}}\right)^2 + 6,961\left(\frac{k_c}{k_{\max}}\right)\right] \tag{65}$$

Magnitude earthquake 7.50 (average values) :

$$\frac{d}{k_{\max}.g.T_0} = \exp\left[-1,86313 - 0,69815Ln\left(\frac{k_c}{k_{\max}}\right) - 7,53273\left(\frac{k_c}{k_{\max}}\right)^2 + 0,95338\left(\frac{k_c}{k_{\max}}\right)\right] \tag{66}$$

Magnitude earthquake 6.50 (average values)

International Journal of Engineering Research & Technology (IJERT)
ISSN: 2278-0181
Vol. 10 Issue 11, November-2021

$$\frac{d}{k_{max}.g.T_0} = \exp\left[-5,334 - 1,610Ln\left(\frac{k_c}{k_{max}}\right) - 10,9785\left(\frac{k_c}{k_{max}}\right)^2 + 7,33983\left(\frac{k_c}{k_{max}}\right)\right] \quad (67)$$

4.2 Implementation of the Method

The implementation of the Simplified Dynamic Method for the dynamic calculation of embankments according to [17], requires the knowledge of:

1. the physical and geometrical characteristics of the Embankment;
2. the dynamic shear strength of the Embankment materials;
3. the fundamental period (or frequency f0) of the embankment (symbol);
4. the value of the critical acceleration (symbol) and the mean cyclic distortion associated with the earthquake;
5. the characteristics of the earthquake;

4.2.1 Fill characteristics

The characteristics of the backfill for the use of the Seed and Makdisi method are: The density of the backfill ρ (measured in situ), the maximum shear modulus of the embankment material G_{max} (obtained from cyclic triaxial tests), the embankment shear modulus G (obtained from geophysical tests) and the embankment height H. These characteristics are illustrated in Figure 9.

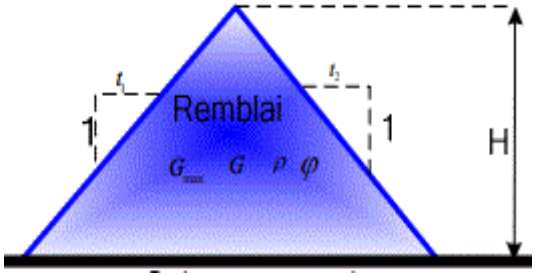

a) triangular fill

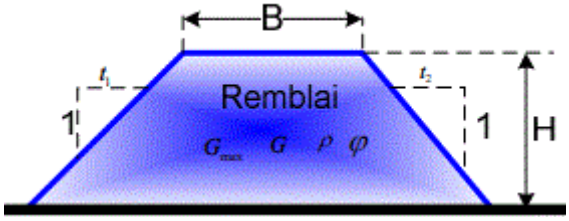

b) trapezoidal fill

Figure 9: Characteristics of an embankment on bedrock

4.2.2 Dynamic shear strength of the embankment

The dynamic shear strength of the embankment soil (obtained from triaxial tests) is determined not only by the evolution of the stress deviator as a function of the number of cycles, but also by the variations of the shear modulus and damping as a function of cyclic deformation or distortion. When using the Seed Makdisi method, only the variations of the normalized shear modulus

International Journal of Engineering Research & Technology (IJERT)
ISSN: 2278-0181
Vol. 10 Issue 11, November-2021

$\frac{G}{G_{max}}$ and the average damping factor λ (%) as a function of the cyclic distortion $\gamma_{cycl}(\%)$ are used.

As an indication, Figures 10 and 11 given by [17], show the variations of shear modulus and damping of gravel and gravelly soils as a function of cyclic distortion.

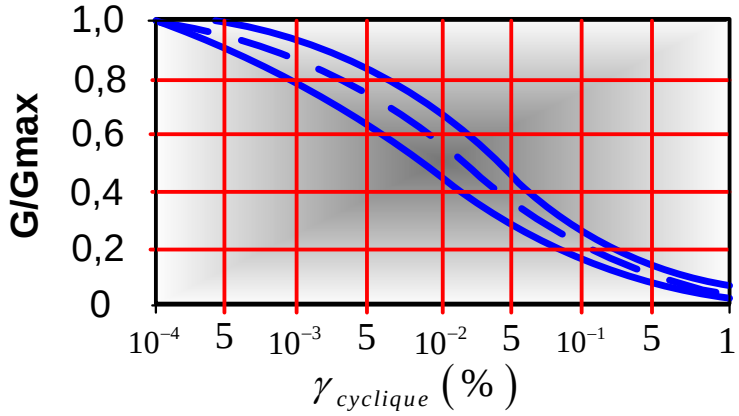

Figure 10: Variation of shear modulus with distortion for gravel and gravelly soils according to [17]

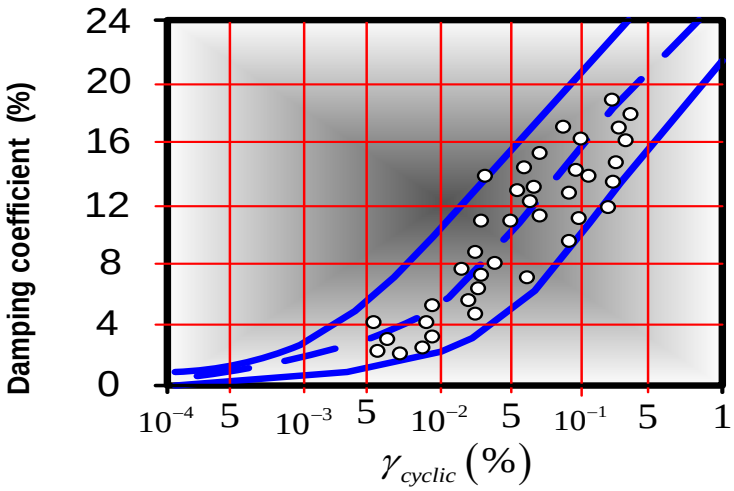

Figure 11: Variation of the damping coefficient with cyclic distortion for sand and gravel soils according to [17]

4.2.3 Basic period first mode T0

For homogeneous fills on bedrock (Figure 9), the fundamental first mode period is according to the formulas (68 or 69) equal to:

$$T_1 = \frac{2\pi H}{\beta_1 \sqrt{\frac{G}{\rho}}} \qquad (68)$$

$$T_1 = \frac{2\pi H}{\beta_1 . V_s} \qquad (69)$$

Where V_s is the shear wave velocity in the embankment. For inhomogeneous fills founded on bedrock, the relationships (70) and

International Journal of Engineering Research & Technology (IJERT)
ISSN: 2278-0181
Vol. 10 Issue 11, November-2021

(71) can be used.

$$T_1 = \frac{2\pi H}{\beta_1 . V_{s_{eq}}} \qquad (70)$$

Where :

$$V_{s_{eq}} = \sqrt{\frac{N}{M}} \qquad (71)$$

with :

$$N = \left[G_1 (t_1 - n_1) + G_2 \left(n_1 + n_2 + \frac{2B}{H} \right) + G_3 (t_2 - n_2) \right] \qquad (72)$$

$$M = \left[\rho_1 (t_1 - n_1) + \rho_2 \left(n_1 + n_2 + \frac{2B}{H} \right) + \rho_3 (t_2 - n_2) \right] \qquad (73)$$

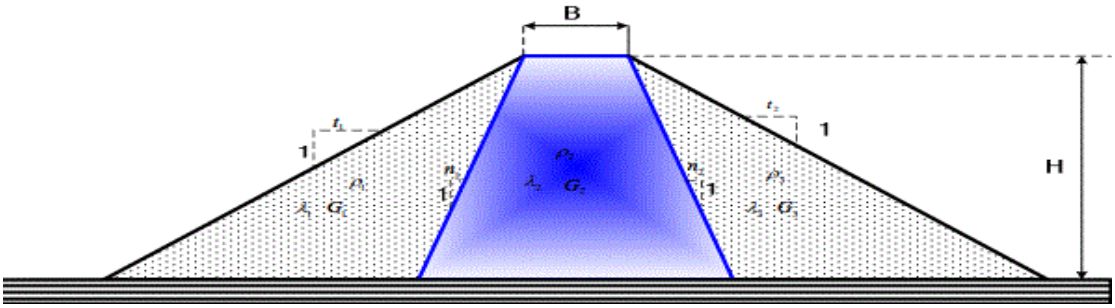

Figure 12: Eigenmodes of zoned dams according to April 1989

For homogeneous embankments not resting directly on bedrock the following relationship can be used to calculate the fundamental period T_0.

$$T_0 = \frac{2\pi H_1}{\bar{a}_1 . V_{s1}} \qquad (74)$$

International Journal of Engineering Research & Technology (IJERT)
ISSN: 2278-0181
Vol. 10 Issue 11, November-2021

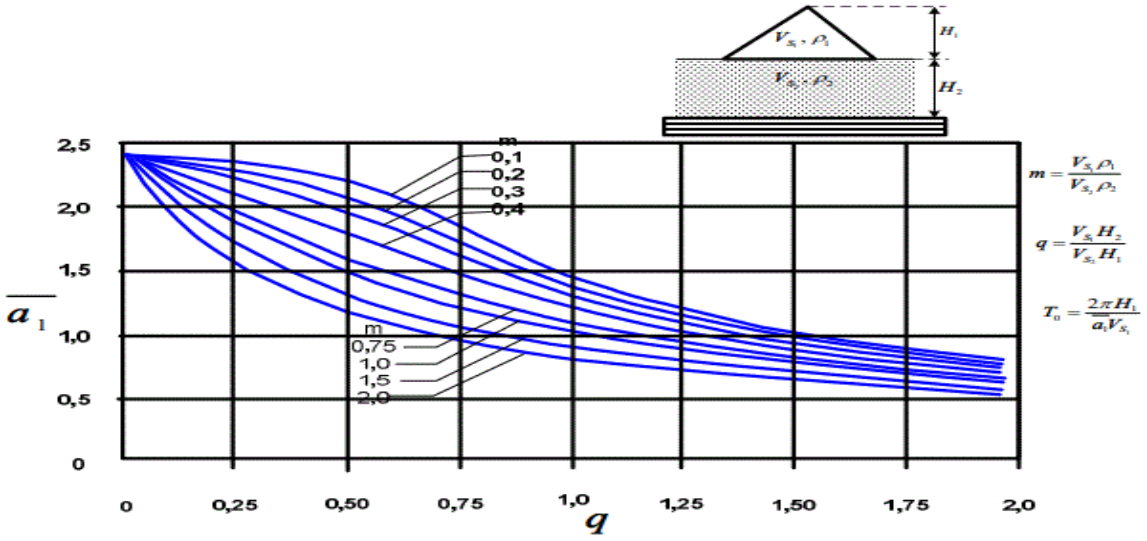

Figure 13: Calculation of the fundamental period of a homogeneous dam resting on an alluvial layer according to [17].

4.2.4 Critical acceleration Kc

The critical acceleration is obtained by pseudo-static analysis methods. It corresponds to the value of seismic acceleration for which the safety coefficient is equal to 1. And the coast (symbol) being the depth at which the failure surface intersects the face of the slope.

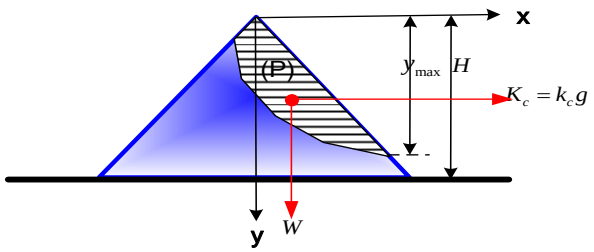

Figure 14: Case of any fracture surface

The critical acceleration coefficient k_c for a flat fracture surface (Figure 15) with a static safety factor F_s is:

$$k_c = (F_s - 1)\tan(\alpha) \tag{75}$$

Where F_s is obtained using expression (76).

$$F_s = \frac{c' L_{AB} + \left(W\cos(\alpha) - u_{AB_{moy}} L_{AB}\right)\tan(\varphi')}{W\sin(\alpha)} \tag{76}$$

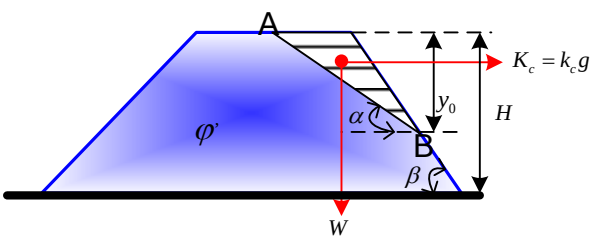

International Journal of Engineering Research & Technology (IJERT)
ISSN: 2278-0181
Vol. 10 Issue 11, November-2021

Figure 15: Case of a flat fracture surface

4.2.5 Earthquake characteristics

The earthquake characteristics are the accelerogram (Figure 19) at the base of the embankment. The acceleration response spectrum $s_\alpha = f(T, \lambda)$ associated with the earthquake which is a function of the damping λ of the embankment material and the period T. This acceleration spectrum s_α is often used in a standard Cartesian representation (Figures 16 and 18), tri-logarithmic (Figure 17) or logarithmic (Figure 20). The spectral acceleration is used to calculate: the maximum cyclic distortion. γ_{cycl}^{eq} (equation 58), the maximum peak acceleration $\ddot{U}_{max}$(relation 57) and the periods T_i corresponding to the "i" mode. We note that, for a given damping, the acceleration spectrum depends on the nature of the soil (Figure 18).

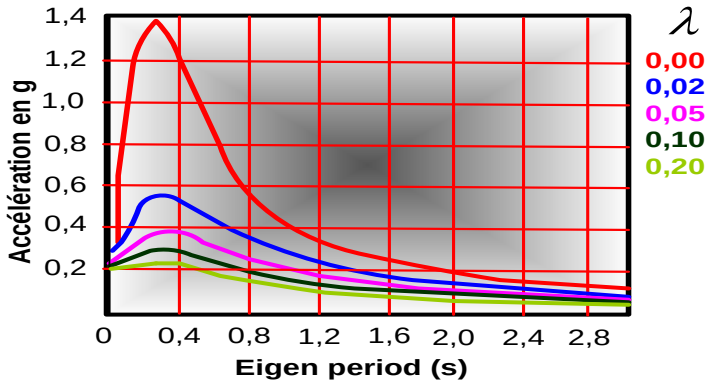

Figure 16: Acceleration spectrum (a_max=0,25g) in Cartesian representation according to [17]

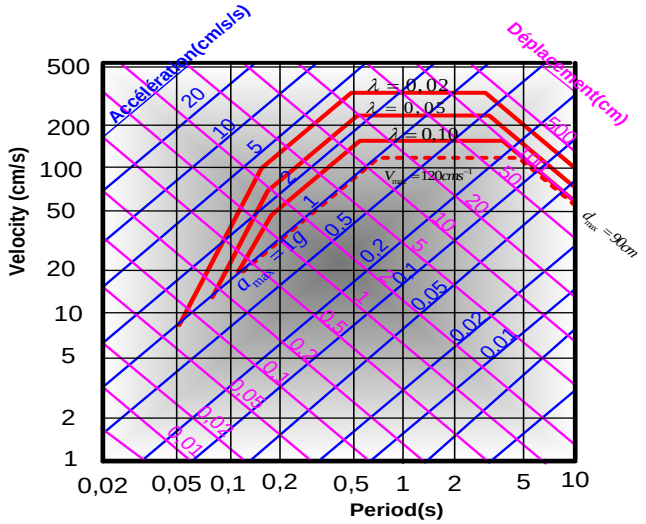

Figure 17: Acceleration spectrum ($a_{max} = 1g$) in cartesian tri-logarithmic representation according [13]

International Journal of Engineering Research & Technology (IJERT)
ISSN: 2278-0181
Vol. 10 Issue 11, November-2021

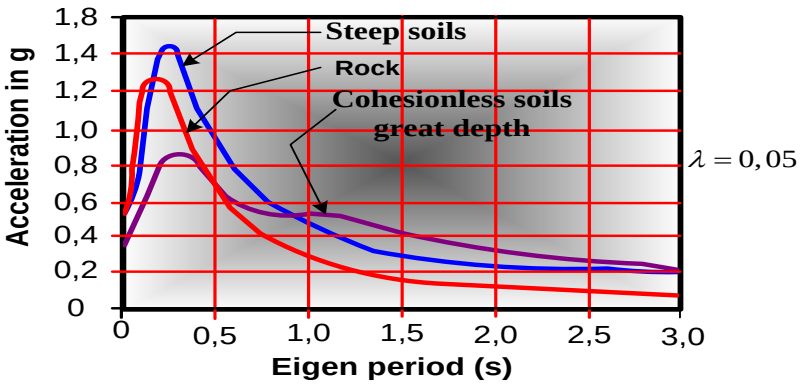

Figure 18: Average spectrum of a magnitude 6.5 earthquake at 8km from the focus for various site conditions according to [17]

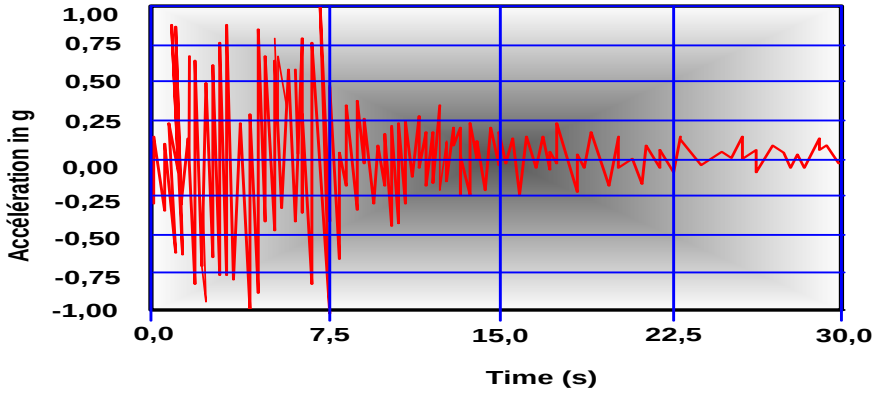

Figure 19: Dynamic calculation of rockfill dams - typical accelerogram according to [9]

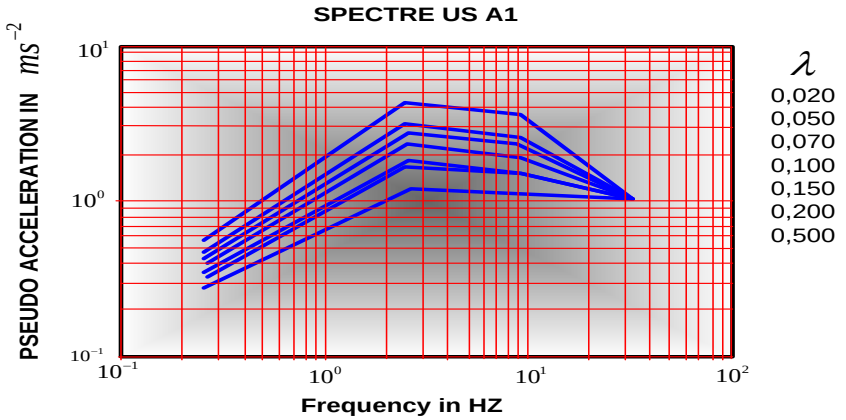

Figure 20: Dynamic calculation of rockfill dams oscillator spectrum (US A1 standards) according to [9].

4.2.6 Calculation of the dynamic characteristics of embankments

The calculation of the dynamic characteristics of the embankment such as peak acceleration and natural periods depends on the average distortion [9] experienced by the structure. This dependence results from the fact that the dynamic shear modulus and damping vary with the distortion (Figures 10 and 11). The calculation procedure, which is summarized in the flowchart in Figure 21, recommends the following steps:

1. Step 1, initial data : $G, K_c, G_{\max}, H, \rho, G = G_{\max} f^{-1}\left(\gamma_{cycl}\right), \lambda = g\left(\gamma_{cycl}\right)$ $S_a = f_1\left(\lambda, T\right) T_n^0$ and $\gamma_{eq}^0 = 0$.

   Step 2, calculate $\frac{G}{G_{max}}$ to derive γ_{eq}^1, λ^1 then calculate $S_{an}^1 = h(\lambda^1, T_n^0)$, $\ddot{U}_{max}^1$

International Journal of Engineering Research & Technology (IJERT)
ISSN: 2278-0181
Vol. 10 Issue 11, November-2021

2. Step 3, we check the condition: $\left|\gamma_{eq}^{i-1} - \gamma_{eq}^{i}\right| \leq \xi = 1$
   - If is not verified, we pose $\gamma_{eq}^{i-1} = \gamma_{eq}^{i}$, we calculate the new values of the G , T_n^i and repeat the procedure in step 2.
   - If is verified, we take$\lambda = \lambda^i$, $T_n = T_n^i$, $\gamma_{eq} = \gamma_{eq}^i$, $\ddot{U}_{max} = \ddot{U}_{max}^1$ and go to step 4.
3. Step 4, the permanent displacements induced by the earthquake are calculated**.**

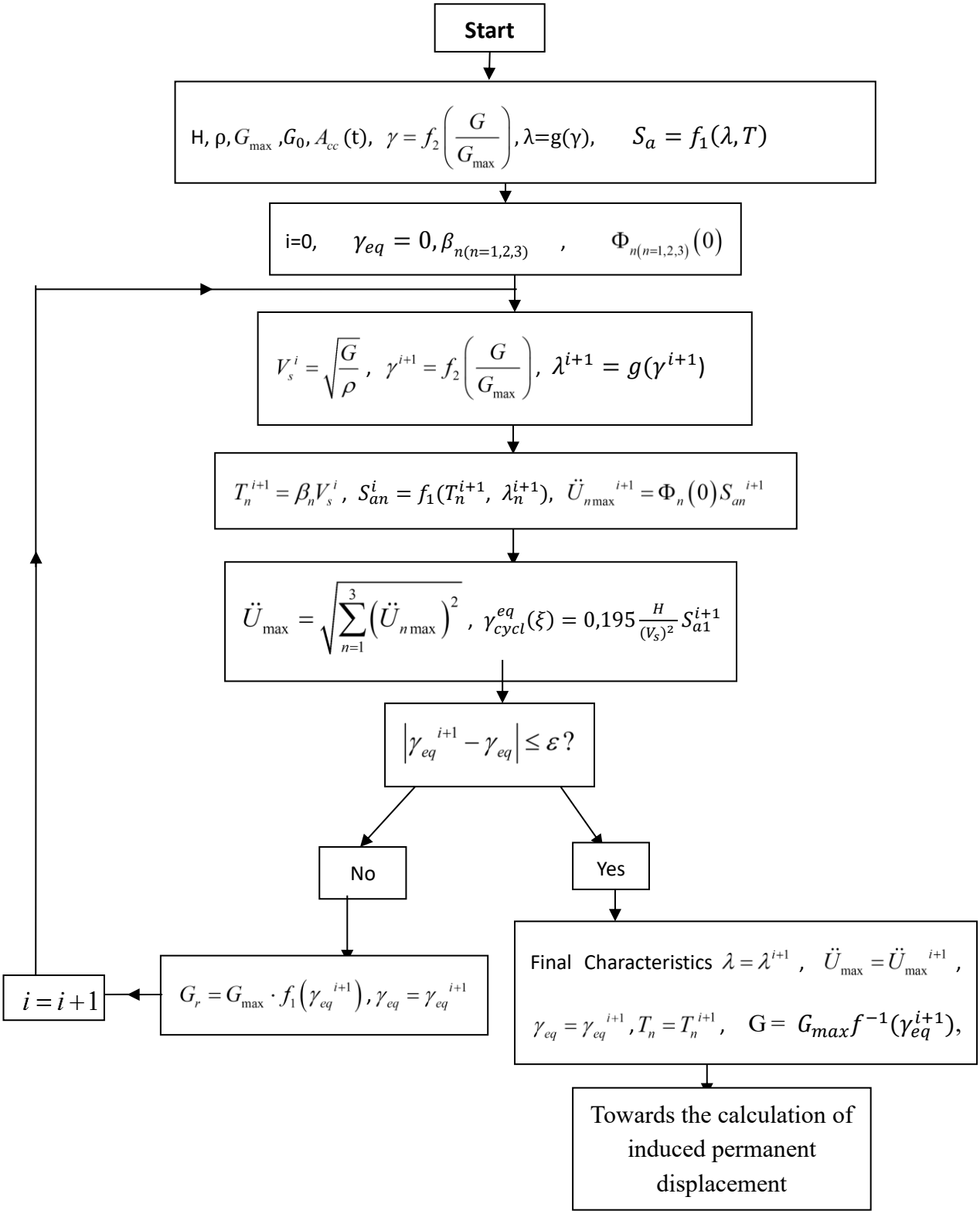

Figure 21: Flow chart for calculation of embankment peak acceleration, natural periods and equivalent cyclic distortion [19].

International Journal of Engineering Research & Technology (IJERT)
ISSN: 2278-0181
Vol. 10 Issue 11, November-2021

4.2.7 Calculation of induced permanent displacements

Knowing the value of the acceleration $\ddot{U}_{max}$ at the crest of the embankment, using the chart in Figure 7, the value of the maximum acceleration coefficient K_{max} of the unstable part of the embankment is determined. Embankment. The ratio $\frac{K_c}{K_{max}}$ is calculated. If this ratio is strictly less than 1, the induced permanent displacements are given by the charts in Figure 8. If this ratio is greater than 1, the embankment is stable and the calculation of the induced permanent displacements is not applicable.

4. APPLICATION

Consider a rockfill dam of 180m height resting on bedrock. The geometric characteristics of this dam are shown in Figure (22). Laboratory tests show that the maximum shear modulus of the dam material is 600MPa, its cohesion is zero and its angle of friction at failure is 40^0. The tests carried out in situ reveal that the shear modulus of the material in place is 216 MPa and its density is The variations of the curves 2T/m^3 and damping $\frac{G}{G_{max}}$ and damping λ(%) as a function of cyclic distortion obtained from the cyclic triaxial tests are equal to the average variations of the curves given by [17] and are illustrated in Figures (10) and (11). The magnitude of the design earthquake is 7,5 on the Richter scale and its maximum acceleration at the base of the structure is equal to 0,25g. The elastic response of the dam is obtained by multiplying the accelerogram spectrum in Figure (16) by an amplification coefficient of 1,6.We evaluate the permanent displacements induced by the design earthquake for the plane failure surfaces given in Figure (22) , all of which pass through point **I** such that IB=11,5m. We draw your attention to the fact that these flat surfaces are not critical failure surfaces for which the safety coefficient and minimum.

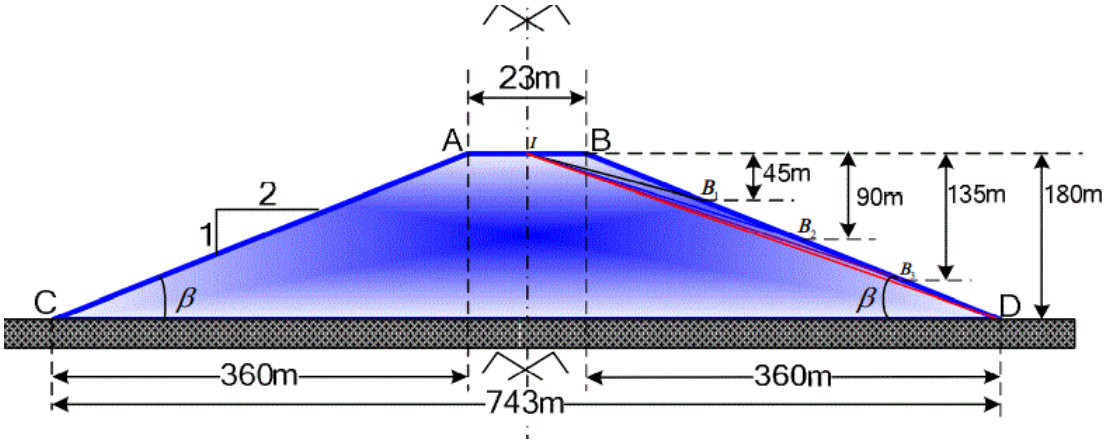

Figure 22: Rockfill dam and slip following flat surfaces

4.1. Maximum acceleration at the embankment crest

The values of the shear modulus G = 216 MPA and the density ρ = 2T/m^3 allow us to calculate the natural periods of the different modes of vibration of the dam which are given in Table 1.

Table 1: Eigen periods of fill mode 1, 2 and 3

Periods	Values
$T_0 = T_1$	1,53s
T_2	0,62s
T_3	0,39s

The application of the flowchart in Figure (21), requires the calculation of the ratio $\frac{G}{G_{max}} = 0{,}36$ which allows us to use the curve in Figure (10) to find the value of cyclic γ_{cycl}= 0,065 % . Moving to Figure (11), we find a damping coefficient λ = 10%. The values of the spectral acceleration S_{ai} associated with the different modes are determined using the curve f(T,λ) (at the Figure (16)) for which λ = 10% . $S_{ai} = 1{,}6 * f(T, \lambda{=}10\%)$ **(77)**

where T_i is the eigenperiod associated with mode 'i'.Using formular (60) and (61), the peak acceleration of the barrage is found to be $\ddot{U}_{max} = 0{,}62g$ and the equivalent distortion obtained $\gamma_{cycl}^{eq} = 0{,}060\ \%$ is very little different from its initial value (0.065%). Using the charts of [20] (average values) or the relations proposed by [19]we obtain the values of the induced permanent displacements "***d***" at different rupture lines which are given in Table 2 and Figure 23.

International Journal of Engineering Research & Technology (IJERT)
ISSN: 2278-0181
Vol. 10 Issue 11, November-2021

Table 2: Permanent displacement '*d*' induced by the magnitude 7.5 earthquake

Blocks	y_{max} (*in meters*)	α	F_s	K_c	y_{max} /H	$\frac{K_{max}}{\ddot{U}_{max}}$	$\ddot{U}_{max}$	K_{max}	$\frac{K_c}{K_{max}}$	T_0	d
IBB_1	45	23,91°	1,57	0,24g	0,25	0,83	0,62g	0,5185g	0,462	1,53s	37,05cm
IBB_2	90	25,17°	1,49	0,213g	0,5	0,62	0,62g	0,366g	0,5823	1,53s	10,98cm
IBB_3	135	25,62°	1,46	0,204g	0,75	0,46	0,62g	0,2562g	0,7949	1,53s	0,89cm
IBB_4	180	25,85°	1,44	0,199g	1,00	0,32	0,62g	0,2013g	0,9874	1,53s	0,05cm

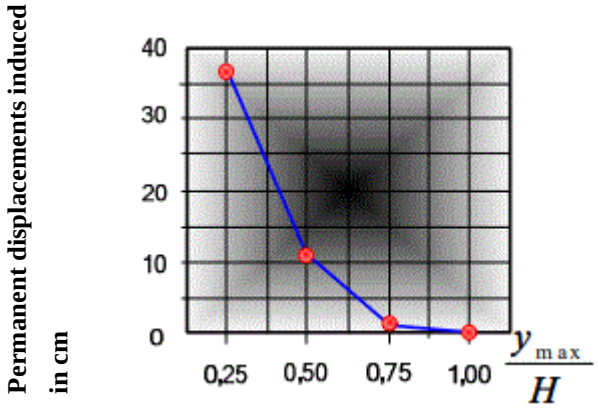

Figure 23: Permanent displacement induced by the Magnitude 7.5 earthquake

From these results, we can see that for flat fracture surfaces, the earthquake-induced permanent displacements decrease as the ratio y_{max}/H increases. Furthermore, we see that the largest displacement obtained is 37cm when $\frac{y_{max}}{H} = 0.25$

5. Conclusions

We have just shown that the simplified dynamic methods in general and in particular that of [20] allow engineers to:

- take into account the effects of earthquakes on embankments or slopes
- calculate the permanent displacements induced along a failure surface in order to verify the second criterion related to the concept of allowable displacements.

However, the implementation of these methods requires that: the foundation soil and the materials constituting the embankment or slope studied must not only verify the non-liquefaction conditions, but also that the shear strength losses recorded at the level of the failure surface are zero or less than 10% of its initial value.

REFERENCES

[1] **Azzouz and Baligh 1983.** Loaded areas on cohesive slopes. Journal of the geotechnical Eng. Division ASCE Vol 109, 1983, GT5 pp. 726-729;
[2] **Biarez J. 1962.** Remarques sur les calculs de stabilité des talus. Annales des Ponts et Chaussées, n0 19 août 1962, p373-393.
[3] **Betrand J. 1987** Méthodes simplifiées de dimensionnement pour barrages en remblais et en enrochements armé. Journées des Etudes EDF calculs dynamiques des barrages ; mars 1987.18pges.
[4] **Caquot A. 1954.** Méthode exacte pour le calcul de la rupture d'un massif par glissement cylindrique. Proc. Eur. Conf. Stockholm. Vol. 1.
[5] **Faure R. M.1982,** Outils numérique en mécanique des sols, application aux stabilités de pentes. Thèse de Doctorat présentée à Paris VI. Mars 1882.
[6] **Frôlich O. K. 1963.** Grundzüge einer Statik der erdböshungen. Der Bauingenieur ,38.
[7] **Helle 1983.** Risque sismique et stabilité des pentes. Application aux barrages. Thèse présentée à l'Université de Grenoble soutenue le 7 juillet 1983 pour obtenir le titre de docteur Ingénieur
[8] **Jambu N. 1954.** Application of composite slip surfaces for stability analysis. Proceedings European Conference of stability earth. Stockholm, Vol. 3.
[9] **Mamba M. 1989.** Résistance au cisaillement des matériaux grossiers applications aux calculs des barrages. Thèse de Doctorat de Génie Civil de

International Journal of Engineering Research & Technology (IJERT)
ISSN: 2278-0181
Vol. 10 Issue 11, November-2021

l'Université de Sciences et Techniques de Lille. 1er Décembre 1989 ; 250 pages.

[10] **Makdisi F. I. and Seed H. B. 1978** Simplified procedure for evaluating embankment responses. Journal of the Geotechnical Engineering Division. Vol. 105, n0 GT12. Dec. pp.1427-1434.30

[11] **Michlowsky 1989,** three dimensional analysis of locally loaded slopes geotechnique 39,1989 n0 1, pp. 27- 38;

[12] **Morgenstern N. R. and Price W.E 1965.** The analysis of stability of general slip surface. Vol. 15.

[13] **Newmark N. M. 1965.** Effects of earthquakes on dams and embankments. J. Geotechnique, 15, n0 2, pp. 139-160.

[14] **Odéon H. 1988 problème posé par la prise** en compte de l'eau dans le calcul de stabilité des Talus. Mémoire de DEA, filière géotechnique et Sciences des matériaux.

[15] **Raulin P. Rouques G., Toubol A. 1974.** Calcul de la stabilité des talus en rupture non circulaire. Rapport de recherche n0 36 des Laboratoires des Ponts et Chaussées Juin 1974.

[16] **Sarma S.K 1981.** Seismic displacement analysis of earth dams. Journal of geotechnical engineering division. Proceedings of America Society of Civil Engineering. Vol. 107 n0 GT12, pp.1735-1739. December.

[17] **Seed H. B and Makdisi F. I. 1978.** Simplified procedure for estimating dam and embankment earthquake induced deformations. Journal of the Geotechnical Engineering Division. ASCE Vol. 104, n0 GT7. pp 849-867; July.

[18] **Seed B. and Martin G.R 1966.** The seismic coefficient in earth dam design. Journal of soil Mechanics and Foundation Division. ASCE, Vol. 92, n0 SM. 3 pp 25-28.

[19] **Skempton A. W 1968.** Stability of earth slopes and embankments foundation. Conf. Int. Meca. Sol Mexico.

[20] **Tatchou Ntemfack M.H 2011**. Mise au point d'un logiciel d'optimisation des talus par les méthodes dynamiques simplifiées. Mémoire de fin d'étude en vue de l'obtention du diplôme d'ingénieur de conception de l'Ecole Polytechnique de Yaoundé saptembre 2011.

[21] **Taylor A. W. 1948.** Fundamentals of soils mechanics. J. Wiley New York 700pges.

[22] **Zhang Xing(1988)** Three dimensional stability analysis of concave slopes in plan view. Journal of the geotechnical engineering. Vol. 114 n0 6 June 1988.